Journal of Materials Chemistry C

Accepted Manuscript

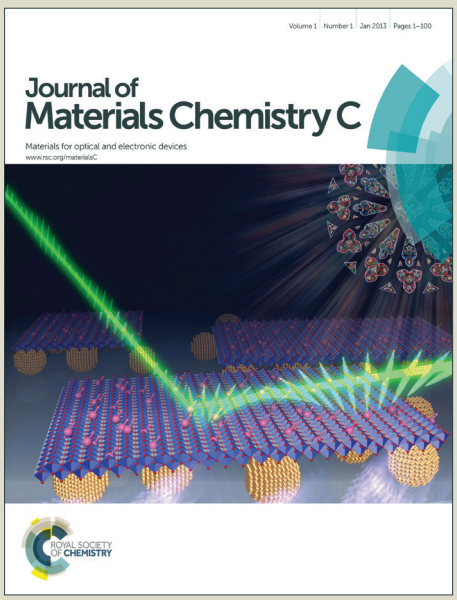

This is an *Accepted Manuscript*, which has been through the Royal Society of Chemistry peer review process and has been accepted for publication.

Accepted Manuscripts are published online shortly after acceptance, before technical editing, formatting and proof reading. Using this free service, authors can make their results available to the community, in citable form, before we publish the edited article. We will replace this *Accepted Manuscript* with the edited and formatted *Advance Article* as soon as it is available.

You can find more information about *Accepted Manuscripts* in the Information for Authors.

Please note that technical editing may introduce minor changes to the text and/or graphics, which may alter content. The journal's standard Terms & Conditions and the Ethical guidelines still apply. In no event shall the Royal Society of Chemistry be held responsible for any errors or omissions in this *Accepted Manuscript* or any consequences arising from the use of any information it contains.

ROYAL SOCIETY OF CHEMISTRY

www.rsc.org/materialsC

Journal of Materials Chemistry C RSCPublishing

FULL PAPER

Tuning the Ambipolar Charge Transport Properties of N-heteropentacenes by Their Frontier Molecular Orbital Energy Levels

Cite this: DOI: 10.1039/x0xx00000x

Received 00th January 2012,
Accepted 00th January 2012

DOI: 10.1039/x0xx00000x

www.rsc.org/MaterialsC

Ke Liu, [a] Cheng-Li Song, [c] Ye-Cheng Zhou, [a] Xing-Yu Zhou, [a] Xiao-Jun Pan, [b] Lu-Ya Cao, [a] Cheng Zhang, [a] Yu Liu, [a] Xiong Gong, [b] and Hao-Li Zhang* [a]

A combined experimental and theoretical study was carried out to investigate the ambipolar charge transport properties of a series of N-heteropentacenes in organic field-effect transistors (OFETs). Introduction of nitrogen atoms in the core and halogen atoms around the periphery of the pentacene framework can efficiently tune the highest occupied molecular orbitals (HOMOs) of the N-heteropentacenes from −5.18 eV to −5.53 eV and the lowest unoccupied molecular orbitals (LUMOs) from −3.08 eV to −3.69 eV. By lowering their HOMO and LUMO energy levels with respect to the Fermi level of the gold electrode, the transistors of these molecules exhibited a transition from hole-dominant bipolar, to balanced ambipolar, and to electron-dominant bipolar transport characteristics. Meanwhile, with the lowering of the frontier molecular orbital energy levels, the transistors also exhibited a decrease of the electron threshold voltage and an increase of the hole threshold voltage. Charge carrier mobility calculation based on Marcus theory and first principle molecular dynamic was conducted to simulate the carrier transport dynamics. The comparison between experimental and theoretical results revealed that for the given device structure, the ratio of electron and hole mobilities of the ambipolar OFETs were strongly affected by the charge injection barrier. This result provides useful guideline for future molecular design for ambipolar OFETs.

1. Introduction

Organic field-effect transistors (OFETs) have attracted great attention from both academic and industrial sectors, as they are featured by light weight, high flexibility, and low-cost in large scale fabrication as alternatives to conventional silicon-based transistor.[1-5] The demand in high performance devices has significantly stimulated the development of new organic semiconductors. In the last decade, large number of organic semiconductors have been developed and utilized for fabrication of high performance OFETs.[6, 7] So far, the majority of organic semiconductors give only unipolar transport characteristics in their OFET devices, *i.e.*, either hole-transport (p-type) or electron-transport (n-type) properties.[8-12] In recent years, there has been a significant growth of interest toward ambipolar organic semiconductors. Ambipolar semiconductors allow both hole and electron to act as the charge carriers, which are important for applications like organic light-emitting transistors and complementary inverter circuits.[3, 13-17]

Several groups have reported that pentacene derivatives possess electron-transport properties[18, 19] when the aromatic framework is attached with high electron affinity moieties.[10, 20, 21] For example, Bao *et al*. have reported that halogenation can convert unipolar p-type pentacene into ambipolar materials.[22, 23] Theoretical simulations by Houk[24] and Ren[25] have suggested that replacing sp^2 carbon atoms with nitrogen may give electron-transport materials. Large number of N-heteroacenes have been synthesized in recent years,[26-29] but only a few have shown appreciable charge carrier mobility.[30, 31] Zhang *et al*. have synthesized various large heteroacenes,[32-36] which possess high performance in photocurrent response,[35] aggregation-induced emission,[33] and memory.[36] Miao has reported an N−heteropentacene exhibiting electron transport mobility up to 1.0~3.3 $cm^2\ V^{-1}\ s^{-1}$.[31] Our group has reported several N-heteropentacenes[30, 37] exhibiting balanced ambipolar transport properties, which can be used in fabrication of high performance complementary inverters using low-cost electrodes.[38] However, the working mechanism of ambipolar OFETs is still not well understood, and very few ambipolar materials have been systematically studied by both theoretical simulations and experimental methods.

In order to achieve the full potential of ambipolar organic semiconductors, it is essential to understand the correlation between the structures and the properties. While the transport properties of many ambipolar semiconductors have been

Journal of Materials Chemistry C Accepted Manuscript

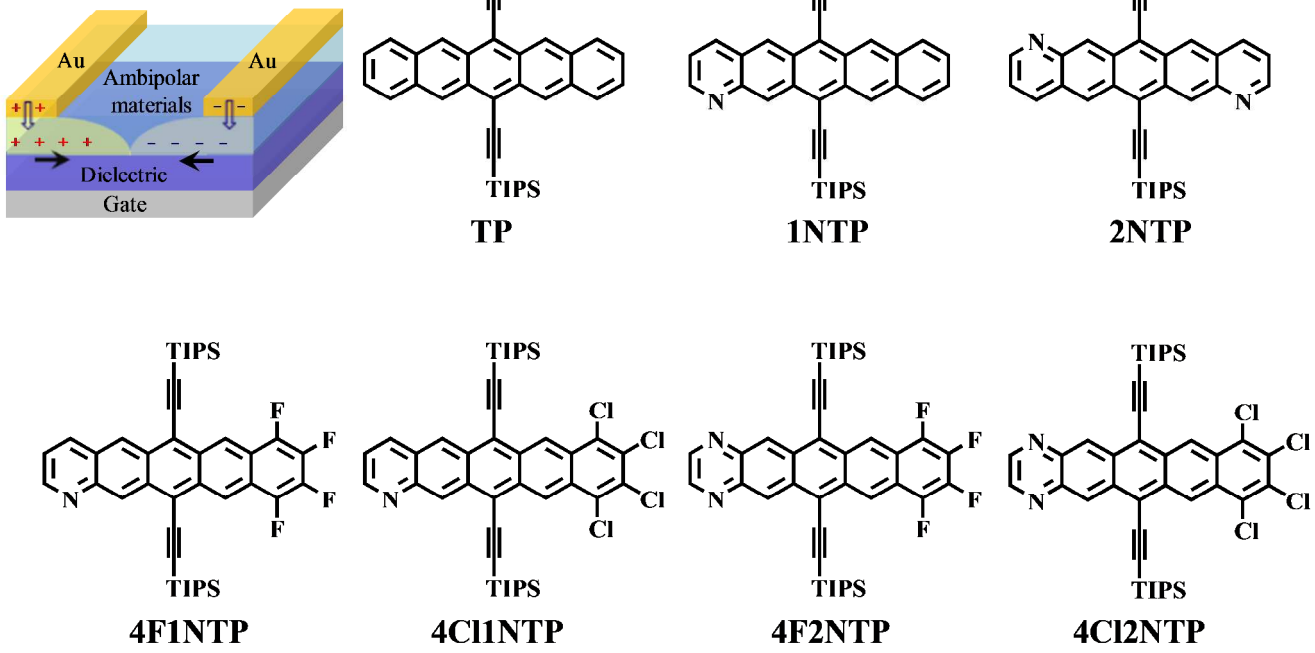

Figure 1. OFET device structure and molecules studied in this work

investigated by various groups, it is not feasible to make structure-property correlation by simply comparing these data from different groups, because the OFET performance is strongly affected by many factors, such as the sample purity and the device fabrication conditions. For example, the reported mobility of the OFETs from 6,13-bis((triisopropylsilyl)ethynyl)pentacene (TP), a widely studied p-type organic semiconductor, varies from 10^{-4} to 4.6 cm^2 V^{-1} s^{-1} by different groups.[7, 39] Therefore, to obtain an accurate correlation between structures and properties of different organic semiconductors, it is crucial to carry out the investigation under the same conditions.

The aim of this research is to identify the factors that affect the hole and electron transport properties of an ambipolar OFET. We focus on two very basic processes, which are the charge injection at the metal/molecule interface and the charge transport within the thin films of organic semiconductors.[40, 41] The charge transport within the active layer of an OFET is strongly influenced by the molecular orientation and packing motif. Recent theoretical studies have indicated that many organic semiconductors are in fact able to transport both hole and electron in their crystalline forms.[3] In reality, the majority of OFET devices have only shown unipolar transport behavior, which can be attributed to that the charge injection barriers at the electrode/molecule interface favor the injection and transport of only one type of charge carriers. In contrast to unipolar transistors, an ambipolar transistor allows both electron and hole to be injected into the organic active layers as well as to transport within the organic layers, so its performance should be affected by both charge injection and transport processes. However there have been very few investigations attempted to identify the roles of the two processes in the ambipolar transistors. Bao has proposed an empirical plot which correlates the carrier type with frontier molecular orbital energy levels.[42] but it's still unclear how the charge injection process affects the device parameters, particularly the values of hole/electron mobility and threshold voltage.

In this work, we have used the N-heteropentacene as a model system to study the effects of the charge injection process and charge transport dynamics on the device performance of ambipolar transistors. The structures of the model molecules are shown in Fig. 1. Molecule TP (also known as Tips-pentacene) is used as a reference in our work, as it is a widely studied p-type material. Two N-heteropentacenes (1NTP, 2NTP) and four halogenated N-heteropentacenes (4F1NTP, 4Cl1NTP, 4F2NTP, and 4Cl2NTP) were studied, among which 4F2NTP and 4Cl2NTP were synthesized for the first time. The thin film transistors were fabricated following the standard procedures, and the charge transport properties of the different transistors were characterized. Great efforts have been made to minimize the potential influences from the other factors, such as sample purity, film growth and device fabrication conditions. The comparison between these compounds could provide insights to the factors that affect the device performance of the ambipolar transistors.

Journal of Materials Chemistry C Accepted Manuscript

This journal is © The Royal Society of Chemistry 2015

2. Results and Discussions

2.1 Spectroscopic and electrochemical properties

We have investigated the energy levels of all the pentacene derivatives in both solutions and thin films. The ultraviolet-visible (UV-vis) absorption spectra and the fluorescence emission spectra of all the compounds are very similar (Supplementary Fig. S1 and Fig. S2). The absorption maximum of all the compounds in toluene solutions were found in the range of 637 to 657 nm. Their absorption maximum in thin films are red shifted by about 20 nm, along with significant peak broadening compared with the absorptions in solution, indicating strong electronic interactions between molecules in the solid state.[43] The calculated optical gaps are very similar for all the compounds. In solution, the optical gaps range from 1.81 to 1.88 eV; while in thin films, the gaps are significantly smaller, which are in the range of 1.47 to 1.62 eV (Tab. 1).

The energy levels of the frontier orbitals, including the highest occupied molecular orbital (HOMO) and the lowest unoccupied molecular orbital (LUMO), of all the N-heteropentacenes were estimated from cyclic voltammetry. The cyclic voltammograms of the N-heteropentacenes in dichloromethane (CH_2Cl_2) solution show very similar features, including two clear reversible redox waves at low potential and one irreversible oxidation wave at high potential (Fig. 2). The completely reversible redox waves at low potential reveal the marked electron-deficiency of these molecules and their potential electron-transporting nature.[44] The cyclic voltammograms confirm that the band gaps of these compounds are quite similar, but their LUMO and HOMO positions are gradually shifted by the different modifications to the pentacene framework. Inserting nitrogen atoms into the core and peripheral halogenation show the effect of lowering the energy levels of the frontier molecular orbitals. All of the N-heteropentacenes exhibited LUMO energies lower than −3.3 eV (Tab. 1), suggesting that they have high electron affinities and are candidates for n-channel semiconductors.[44, 45] Miao has indicated that inserting N atoms into the 2nd and 4th rings of the pentacene framework has more significant energy level lowering effect compared to modification to the 1st and 5th rings.[21] In our work, we have only modified the 1st and 5th rings, since this modification gives finer control to the energy levels. Meanwhile, it is noticed that the LUMO levels of the chlorinated compounds 4Cl1NTP (−3.53 eV) and 4Cl2NTP (−3.69 eV) are lower than that of their fluorinated counterparts 4F1NTP (−3.46 eV) and 4F2NTP (−3.61 eV), even though Cl is less electronegative than F. This phenomenon is attributed to the conjugation effects from the Cl empty 3d orbitals, which is consistent with Bao' report on other chloroacenes[23] and our previous research.[46] Compared to 4F1NTP and 4Cl1NTP, 4F2NTP and 4Cl2NTP show much lower LUMO energies. Meanwhile, we also noted that not only the LUMO positions are gradually lowered, but also the HOMO positions are lowered by the nitrogen and halogen substitution as well, so that the energy gaps of all the molecules remain nearly unchanged.

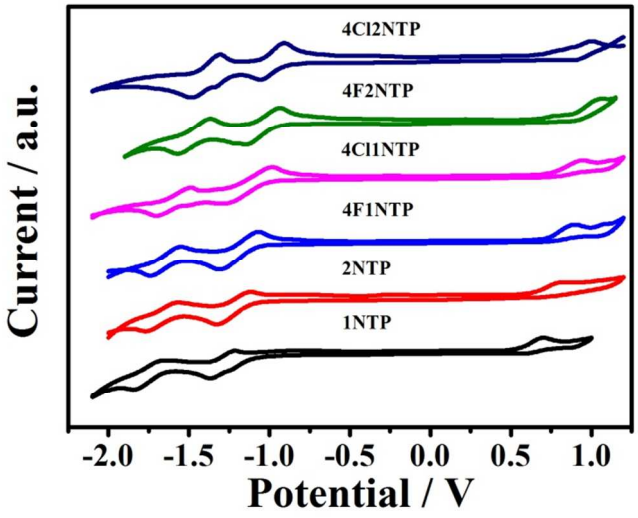

Figure 2. Cyclic voltammograms of all the N-heteropentacene derivatives in CH_2Cl_2 in 0.1 M Bu_4NBF_4 at a scan rate of 100 mV s^{-1}, with respect to a $FeCp_2^+/FeCp_2^0$ reference (−4.8 eV to vacuum) added after each measurement.

Table 1. Summary of optical, electrochemical and DFT-MO theoretical calculated energy levels (eV) of the different compounds.[30, 37]

Mol.	UV-vis		[c]CVs			[d]DFT		
	[a]E_g^{sol}	[b]E_g^{film}	E_{LUMO}	E_{HOMO}	E_g	E_{LUMO}	E_{HOMO}	E_g
TP	1.87	1.58	−3.08	−5.18	2.10	−3.05	−4.95	1.90
1NTP	1.86	1.58	−3.33	−5.31	1.98	−3.17	−5.07	1.90
2NTP	1.88	1.62	−3.40	−5.42	2.02	−3.27	−5.19	1.92
4F1NTP	1.88	1.55	−3.46	−5.49	2.03	−3.48	−5.39	1.91
4Cl1NTP	1.85	1.47	−3.53	−5.50	1.97	−3.51	−5.39	1.88
4F2NTP	1.83	1.49	−3.61	−5.51	1.90	−3.53	−5.40	1.87
4Cl2NTP	1.81	1.49	−3.69	−5.53	1.84	−3.61	−5.47	1.86

[a] Band gaps estimated from UV-vis absorption edge in solution. [b] Band gaps estimated from UV-vis absorption edge of about 50 nm thin films on quartz. [c]0.1 M Bu_4NBF_4 in CH_2Cl_2 at a scan rate of 100 mV/s. $FeCp_2^+/FeCp_2^0$ (-4.8 eV to vacuum) as the internal reference. Extracted $E_{1/2}$ values vs. Fc^+/Fc. LUMO and HOMO energies determined from the equations[31, 35]: E_{LUMO} =-4.80-$E_{1/2}^{red}$ (eV); E_{HOMO} =-4.80-$E_{1/2}^{ox}$ (eV). [d] The theoretical LUMO, HOMO levels and energy gaps were obtained by DFT calculation with B3LYP/6-31G(d) using the Gaussian 09 package. All values are given in eV.

Journal of Materials Chemistry C Accepted Manuscript

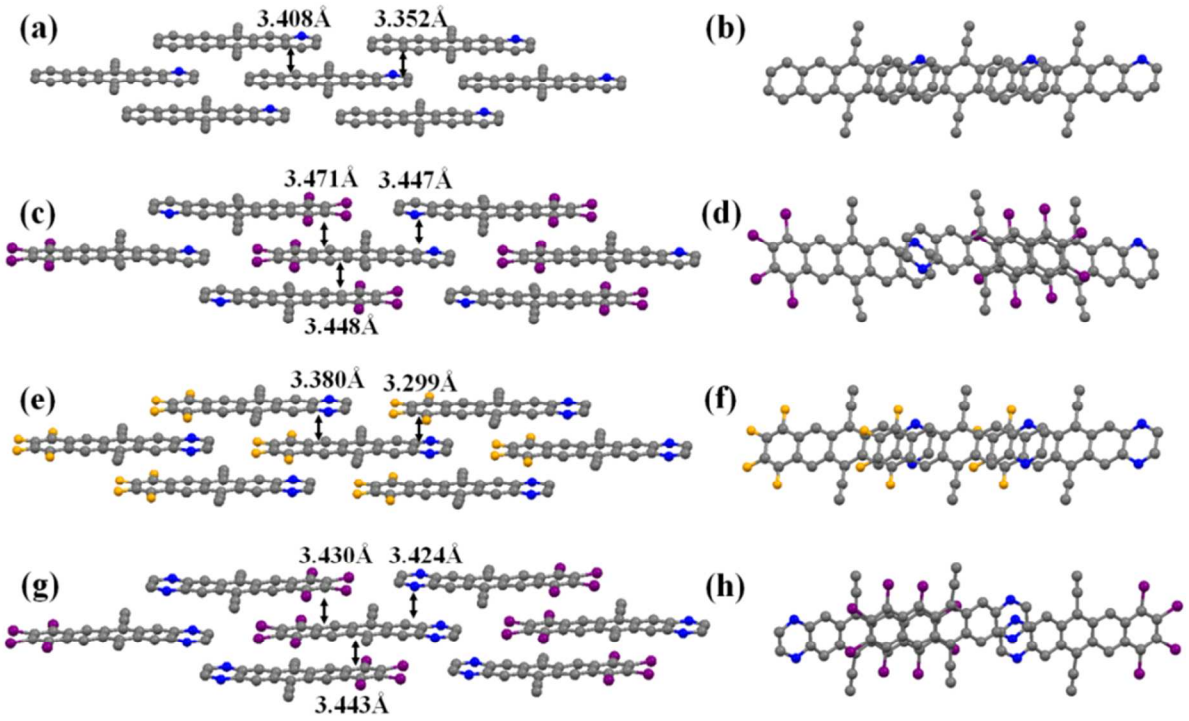

Figure 3. Solid-state arrangement of 1NTP (CCDC 986801), 4Cl1NTP (CCDC 986802), 4F2NTP (CCDC 986803) and 4Cl2NTP (CCDC 986804) in their single crystals. The N atoms are shown in blue and the F in orange, Cl in purple. (a), (c), (e) and (g) view along the axis that is formed by two ethynyl substituents, which does not correspond to any crystallographic axis. (b), (d), (f) and (h) view along the a-axis, which shows significant overlap between stacks.

The energy gaps of the N-heteropentacenes calculated by density functional theory (DFT) method, are in excellent agreement with those obtained by the cyclic voltammetry measurements, confirming the experimental observation that all the N-heteropentacenes display very similar HOMO–LUMO gaps, but the LUMO and HOMO positions are gradually lowered by incorporating more nitrogen atoms or (and) halogen substitutions.

The six N-heteropentacene molecules exhibit much higher photo-stability compared to TP, which is attributed to their lower HOMO levels (Supplementary Fig. S3a). The observed photo-stability of these molecules followed the order of 4Cl2NTP ≈ 4F2NTP > 4Cl1NTP ≈ 4F1NTP > 2NTP > 1NTP > TP. The N-heteropentacene compounds also showed very high decomposition temperatures exceeding 350 °C (Supplementary Fig. S3b). The good stability of the N-heteropentacenes allows the field-effect transistors to be prepared by thermally deposition method.

2.2 Single-crystal structure

The crystal structures of 2NTP and 4F1NTP have been reported in our previous work.[30] The crystal structures of 1NTP, 4Cl1NTP, 4F2NTP and 4Cl2NTP are shown in Fig. 3. In the solid states, the N-heteropentacene units of the six molecules display near-perfect flat stacking and exhibit significant π-π intermolecular overlaps, which are ideal for charge carrier transport between molecules. Most apparently, none of the compounds adopts the herringbone pattern of pentacene. Instead, they stack with a brickwork motif with significant overlap of the aromatic rings between the adjacent molecules.[47] It is observed that the single crystals of all of the N-heteropentacenes showed similar molecular packing motif. The distance between the π-stacks of adjacent molecules are 3.352 Å, 3.345 Å, 3.298 Å, 3.447 Å, 3.299 Å and 3.424 Å in the 1NTP, 2NTP, 4F1NTP, 4Cl1NTP, 4F2NTP and 4Cl2NTP respectively. The distances are very close to the interplanar distance in graphite (3.40 Å). The distances of π-stacking between intermolecular contacts are very close to van der Waals radii between neighboring stacks. Meanwhile, X-ray diffraction (XRD) patterns of the thin films of all pentacene derivatives show similar intermolecular orientation (Supplementary Fig. S4, and Tab. S1). Fig. S5 shows the atomic force microscope (AFM) images of the thin films of all pentacene derivatives. The thin film morphologies of all the samples share some similarities including ordered microstructure with terraced surface, which could be attributed to their similar structure and molecular packing in crystals. To investigate these issues in greater depth, the packing patterns from the thin films of three representative molecules (1NTP, 2NTP and 4Cl1NTP) were investigated by two-dimensional grazing incident X-ray diffraction (2D-GIXRD) using synchrotron X-ray source (as shown in Fig. S6). These results showed a large number of well-defined diffraction peaks, which indicates a high degree of crystalline order, in accordance with the XRD patterns.

Journal of Materials Chemistry C Accepted Manuscript

This journal is © The Royal Society of Chemistry 2015

2.3 OFET device fabrication and characterization

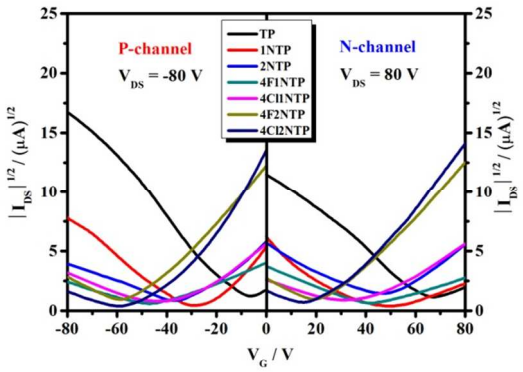

Figure 4. Typical p-channel (left) transfer curves and n-channel (right) transfer curves for all N-heteropentacene derivatives deposited on OTMS-treated SiO_2 substrates at T_{sub} = 60 °C with Au electrodes.

The typical transfer curves for the thin films transistors of all the pentacene derivatives deposited on octadecyltrimethoxysilane (OTMS)-modified SiO_2 dielectric with Au electrodes are shown in Fig. 4 (the typical output curves are shown in Supplementary Fig. S7). The OFETs were prepared at substrate temperature T_{sub} =60 °C. Also, we have employed a slow deposition rate, below 0.1 Å/s. It is found that all of the transistors exhibit ambipolar transport properties, *i.e.,* both p-channel (left) transfer curves and n-channel (right) transfer curves can be observed.

Tab. 2 compares the OFET performance of all of the pentacene derivatives. The mobilities and threshold voltages reported in this table are averages from at least 20 OFETs.

Table 2. Summary of the average experimental mobilities (μ), ratios of electron and hole mobilities (μ_e/μ_h), and average threshold voltages (V_{th}) of top-contact OFET devices fabricated for all the pentacene derivatives on OTMS-modified SiO_2 dielectric at T_{sub} = 60 °C with W/L of 20 (W = 3000 μm, L = 150 μm) (Au electrodes).

Material	μ/cm^2 V^{-1} s^{-1}			V_{th}/V	
	μ_h	μ_e	μ_e/μ_h	h	e
TP	0.95±0.06	0.05±0.02	0.05	−10±3	+60±4
1NTP	0.42±0.07	0.10±0.02	0.24	−28±5	+50±4
2NTP	0.30±0.05	0.20±0.09	0.67	−32±6	+43±8
4F1NTP	0.12±0.02	0.11±0.03	0.92	−40±2	+40±2
4Cl1NTP	0.20±0.03	0.22±0.02	1.10	−42±3	+35±3
4F2NTP	0.14±0.04	0.57±0.02	4.07	−54±4	+20±4
4Cl2NTP	0.07±0.03	0.83±0.04	11.86	−59±3	+16±5

The mobilities and threshold voltages reported in this table are averages from at least 20 OFETs.

In our previous works,[30, 37] we have reported preliminary results regarding the transistor performance of the compounds 1NTP, 2NTP, 4F1NTP and 4Cl1NTP. In this work, these compounds give improved device performance compared to that reported previously due to higher sample purity and optimized device fabrication conditions.[30, 37] It is noticeable that the mobility increase is higher for hole (μ_h) than for electron (μ_e), which can be attributed to the fact that that electron transport is more easily affected by charge trapping effect than the hole and hence are more difficult to be improved.[3, 10] For the first time, we observed ambipolar transport behavior from the transistor of TP. TP exhibited good hole transport property, with the hole mobility reaching 0.95 cm^2 V^{-1} s^{-1}, while its electron mobility was only 0.05 cm^2 V^{-1} s^{-1}, one order of magnitude lower than the hole mobility. In our previous work, we only observed hole transport behavior of 1NTP. Herein, 1NTP showed ambipolar properties with the hole mobility (0.42 cm^2 V^{-1} s^{-1}) higher than the electron mobility (0.10 cm^2 V^{-1} s^{-1}). It has been noted by many researchers that the charge trapping effect is more sensitive against the electrons than the holes,[3, 10] and electrons are more likely to be trapped by impurities or defects. Compared to 1NTP, 2NTP exhibited higher electron transport properties, with μ_h = 0.30 cm^2 V^{-1} s^{-1} and μ_e = 0.20 cm^2 V^{-1} s^{-1}. The introduction of electronegative N-atoms in the pentacene backbone could efficiently increase the electron transport properties, and consequently induce ambipolar transport properties. 4F1NTP and 4Cl1NTP showed very balanced ambipolar properties. The electron mobility and hole mobility were both very high, with μ_h = 0.12 cm^2 V^{-1} s^{-1}, μ_e = 0.11 cm^2 V^{-1} s^{-1} for 4F1NTP and μ_h = 0.20 cm^2 V^{-1} s^{-1}, μ_e = 0.22 cm^2 V^{-1} s^{-1} for 4Cl1NTP respectively, which were improved from our previous report.[30] The improvement of the mobility value from 4Cl1NTP in this work is mainly attributed to the improved sample purity and film crystallinity, which is confirmed by the XRD results. 4F2NTP also showed ambipolar properties, but the electron mobility (0.57 cm^2 V^{-1} s^{-1}) was higher than the hole mobility (0.14 cm^2 V^{-1} s^{-1}). 4Cl2NTP exhibited good electron transport property, whose electron mobility reached up to 0.83 cm^2 V^{-1} s^{-1}, but almost no hole mobility was observed (one order of magnitude lower than its electron mobility).

Journal of Materials Chemistry C Accepted Manuscript

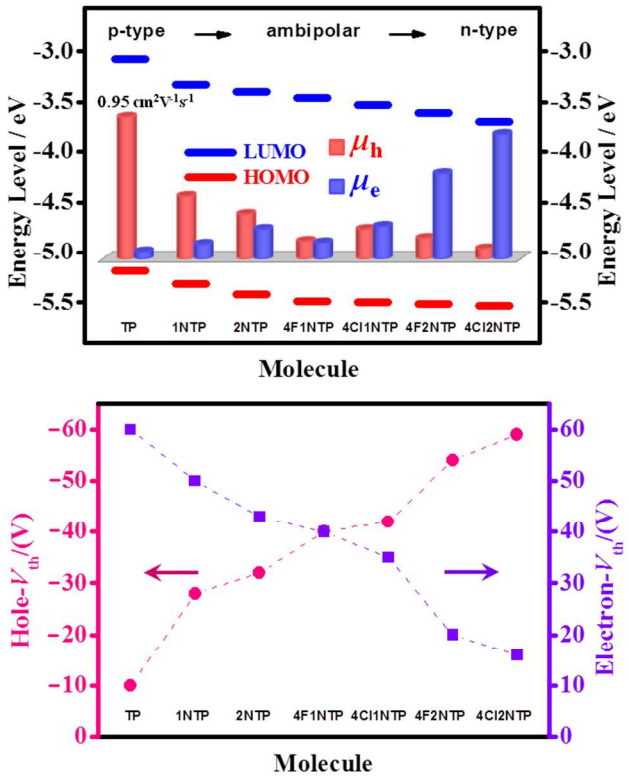

Figure 5. The measured HOMO and LUMO levels, average mobilities (above) and average threshold voltages (below) of electron and hole at T_{sub} = 60 °C with Au electrodes for TP, 1NTP, 2NTP, 4F1NTP, 4Cl1NTP, 4F2NTP and 4Cl2NTP.

Fig. 5 illustrates the correlation between the frontier molecular orbital energy levels and the device performance. It can be seen that with the simultaneous lowering of the molecular orbital energy levels, the semiconductor materials changed from hole-dominant bipolar, to balanced ambipolar, and to electron-dominant bipolar. This trend is clearly evident by the increasing of the electron/hole mobility ratios (μ_e/μ_h) (Tab. 2). When the Au electrode is used, TP is known as a typical p-type material, whose HOMO and LUMO levels are −5.18 eV and −3.08 eV respectively. When a −CH motif of TP is replaced by an N-atom (1NTP), the LUMO level descends to −3.33 eV, and the molecule is converted to a weak ambipolar material, though the low μ_e/μ_h ratio of 0.24 indicates that p-type property predominates. In 2NTP, with two nitrogen atoms incorporated into the core, the μ_e/μ_h ratio increases to an appreciable value of 0.67. Further reduction of the LUMO levels beyond that of 2NTP is achieved by substituting the hydrogen atoms on the terminal benzene ring of 1NTP with F or Cl atoms. Both 4F1NTP and 4Cl1NTP showed μ_e/μ_h ratios close to 1, indicating very balanced ambipolar behavior. When one N-atom is introduced into the 4F1NTP and 4Cl1NTP skeleton, the μ_e/μ_h ratio increased to 4.07 and 11.86, which can be attributed to their much lower LUMO energy levels.

It is important to note that high mobility is not the only criteria required for a high-performance transistor. The control of the threshold voltage and the reduction of the sub-threshold current are also important factors to ensure a low-voltage operative transistor.[48] The threshold voltage (V_{th}) is a measure of the amount of charge that is induce electrostatically in order to switch-on electrical conduction in an OFET. The magnitude of the field-effect threshold voltage depends on several factors, including the density of charge traps on the interface between the organic active layer and the gate dielectric, the quality of the source/drain contacts, and the absence/presence of a "built-in" conduction channel.[49] Herein, we have also studied the changes of the threshold voltage for hole and electron. Interestingly, from compounds TP to 4Cl2NTP, the hole threshold voltage rises from 10 V to 59 V while electron threshold voltage decreases from 60 V to 16 V, which is consistent nicely with the mobility variation tend. This result suggests that the hole and electron threshold voltages are also tuned by the HOMO and LUMO positions of the materials.

Given the similarity of the molecules and the fact that all the OFET devices were fabricated and characterized under the same conditions, we can assume that there're no dramatic differences in the density of traps and crystalline quality of the active layers for the devices studied in this work. The variation of threshold voltage is mainly attributed to the difference in injection barrier height between the metal electrode and organic semiconductor. In a transistor, upon reaching the threshold voltage, it is essential that injection barriers are skipped then charges are injected. A lower LUMO level could lead to a lower electron injection barrier resulted in a lower electron threshold voltage. On the contrary, a lower HOMO level leads to a higher hole injection barrier related with a high hole threshold voltage.[44, 50] Therefore, from TP to 4Cl2NTP, with the lowering of their frontier orbital energy levels, the hole threshold voltage increased and electron threshold voltage decreased, significantly.

3. Theoretical investigation

We have performed theoretical simulation to gain more quantitative understanding of the carrier transport properties in these ambipolar OFETs. The carrier transport within the thin film of organic semiconductors is generally described by the hopping mechanism.[4, 51, 52] It is known from previous researches that a variety of factors could affect the hopping process,[53, 54] such as the reorganization energies of the molecules, electronic couplings between neighboring molecules, driving forces and thin film morphology. Among these factors, the reorganization energy and molecular couplings are strongly dependent on the molecular structure and their packing motif, while the other factors are somehow related to the device fabrication conditions.

Despite the fast development of theoretical simulation methodology in recent years, the exact evaluation of the charge carrier dynamics within the active layer of a real transistor is still challenging at the moment. In this work, we have studied the hopping process of all the pentacene derivatives under two extreme conditions that are in single crystals and in disordered films. The single crystal simulation assumes that the molecules take their single crystal structure and there is no defect. Fig. S9

Journal of Materials Chemistry C Accepted Manuscript

This journal is © The Royal Society of Chemistry 2015

shows the main charge hopping pathways used in the mobility simulation for the single crystal structures of different molecules. Meanwhile, considering that disordered structures, such as defects and grain boundaries, existed in the thin films, we have also simulated the mobility based on disordered films. In such simulations, the amorphous thin films of all the molecules were constructed by using Metropolis Monte Carlo method[55] similar to that described by Kwiatkowski[56] and Andrienko[57] (as shown in Supplementary Fig. S11), and their mobilities were then calculated using the same model as that for the single crystal structures.

Table 3. Summary of the electron and hole simulated mobilities (μ_e and μ_h, $cm^2 V^{-1} s^{-1}$), and mobility ratios (μ_e/μ_h) based on single crystals and disordered films for all the pentacene derivatives.

Material	Single crystals			Disordered films		
	μ_h	μ_e	μ_e/μ_h	μ_h	μ_e	μ_e/μ_h
TP	0.13	2.37	18.23	1.95×10^{-2}	9.41×10^{-3}	0.48
1NTP	0.06	2.16	36.00	3.79×10^{-2}	2.53×10^{-2}	0.67
2NTP	0.14	2.37	16.93	1.71×10^{-2}	2.00×10^{-2}	1.17
4F1NTP	0.03	0.59	19.67	1.54×10^{-2}	1.32×10^{-2}	0.86
4Cl1NTP	1.05	0.54	0.51	5.50×10^{-3}	8.83×10^{-3}	1.61
4F2NTP	0.03	1.39	46.33	2.90×10^{-2}	1.44×10^{-2}	0.50
4Cl2NTP	0.46	0.83	1.80	5.32×10^{-3}	6.53×10^{-3}	1.23

The simulation model to obtain the carrier mobility is based on the first principles quantum mechanics (QM) calculations combined with Marcus theory.[58, 59] Briefly, the transfer integral and reorganization energy are calculated using DFT methods.[24, 60-62] Charge mobility is then obtained by simulating a diffusion process and using the Einstein relationship.[58, 59, 63] We view each hopping event as a nonadiabatic electron-transfer reaction and use standard Marcus theory to express the rate of charge motion between neighboring molecules, the electronic hopping rate (W) is given by the Marcus equation:

$$W = \frac{V^2}{\hbar}\left(\frac{\pi}{\lambda k_B T}\right)^{1/2} \exp\left(-\frac{\lambda}{4k_B T}\right) \quad (1)$$

where V is the electronic couplings between neighboring molecules in the organic single crystal, λ is the reorganization energy, T is the temperature, and k_B is the Boltzmann constant. Then, a diffusion simulation is performed using W as hoping rate between each dimer. The carrier diffusion constant (D) can then be obtained, and from which we obtained mobility through Einstein formula ($\mu = \frac{eD}{k_B T}$). More detailed simulation procedure is available as Supporting Information (Tab. S2, Tab.S3 and Fig. S8 to S12).

The theoretical mobilities of all the patacene derivatives, in both single crystal and disordered film structures, are listed in Tab. 3. The simulation reveals that all the materials facilitate both electron and hole transport within their single crystals and disordered films.[64] The simulated mobilities for single crystals are generally higher than that for disordered films by at least two orders of magnitude. Such result is expected as disorder in active layer will significantly reduce the carrier transport dynamics. However, given that our transistors were based on polycrystalline thin films, it is believed that the simulation based-on disordered films may provide a more realistic description to the carrier transport behavior in our real devices. The calculated μ_e/μ_h ratios for the single crystals exhibit significant discrepancy with the experimental results (Tab. 2 and Tab. 3). In fact, such big discrepancy between theoretical and experimental results is common in the literatures,[65, 66] as charge carrier dynamics in real polycrystalline OFETs devices is far more complex than that in single crystals.

The simulation results for the disordered films show a general increasing trend of μ_e/μ_h ratio from TP to 4Cl2NTP. In another word, such simulation is consistent with the experimental results in the aspect that the introduction of more electron affinitive atoms, *i.e.*, N, Cl and F, to the pentacene framework increases electron mobility in their thin films (Tab. 2 and Tab. 3). For example, the thin film of TP is predicted to have a μ_e/μ_h ratio of 0.48, and the ratio increases to 1.23 for 4Cl2NTP. On the other hand, 4Cl1NTP has the highest μ_e/μ_h ratio of 1.61, while 4F2NTP gives a relatively low μ_e/μ_h ratio of 0.50, consistent with the earlier argument that Cl is more efficient than F to promote electron transport.

It is noticed that the simulated mobilities for disordered structures still showed obvious discrepancy when compared with the experimental results (Tab. 2 and Tab. 3). The change of experimental μ_e/μ_h ratio is much more dramatic than that expected from the simulation. For instance, the transistor of 4Cl2NTP shows a μ_e/μ_h ratio of 11.86, which is almost one magnitude higher than that expected from the theoretical simulation (1.23). Meanwhile, from TP to 4Cl2NTP, the simulated μ_e/μ_h value of the disordered films changes from 0.48 to 1.23, a nearly three-fold increase. In contrast, the

Journal of Materials Chemistry C Accepted Manuscript

experimental μ_e/μ_h value increases 237 times, from 0.05 to 11.86.

We note that the above theoretical simulation based on Marcus theory and first principle molecular dynamic only simulates carrier transport dynamics within the organic semiconductor layer, and does not take into account the charge injection process at the metal/organic semiconductor interface. As the above theoretical simulation results show significant difference with the experimental results, it reveals that the ambipolar transport characteristics of the N-heteropentacenes are unlikely to be solely affected by the hopping-type carrier transport dynamics. Combined with our experimental observation of the strong correlation between the frontier molecular orbital energy levels and the ratio of the electron/hole mobilities (Fig. 5), all these results indicate that the ambipolar transport characteristics of the N-heteropentacenes are strongly affected by the charge injection barrier.

4. Conclusion

We have studied the device performance of field-effect transistors fabricated from a series of N-heteropentacene derivatives. By introducing electronegative nitrogen atom to the pentacene backbone and halogens around the periphery, we simultaneously lowered the LUMO and HOMO, with smaller than 0.1 eV intervals. With the lowering of the injection barriers, the N-heteropentacenes exhibited a transition from hole-dominant bipolar, to balanced ambipolar, and to electron-dominant bipolar transport characteristics. Meanwhile, the electron and hole threshold voltage also changed accordingly with the electron and hole injection barrier. This result suggests that the charge injection barrier strongly affects the change trend of the experimental μ_e/μ_h values in ambipolar OFETs. We suggest that the ideal ambipolar organic semiconductors should meet three key criteria. First, a relatively small LUMO-HOMO gap is required for achieving small injection barriers for both hole and electron. Second, the LUMO and HOMO need to be located at appropriate positions with respect to the metal Fermi level to give balanced electron and hole injection barriers for achieving highly balanced carrier mobilities. Third, their molecular packing in thin film should favor both hole and electron transport.

Our work also indicates that the theoretical simulation based solely on the electron hopping process are not sufficient to describe the device performance of ambipolar OFETs, and further developments of theoretical toolboxes to include the charge injection process are necessary for studying ambipolar organic electronics. It is believed these new understandings provide important guidance to the further design of high performance ambipolar organic semiconductors and investigation of their charge transport properties.

5. Experimental Methods

5.1 Cyclic voltammetry

Cyclic voltammetry (CV) measurements were run on a CHI660B electrochemistry station (CHI, USA) in anhydrous CH_2Cl_2 solution with 0.1 M tetrabutylammonium tetrafluoroborate (Bu_4NBF_4) as the supporting electrolyte, at a scan rate of 100 mV s^{-1}, which is conducted by using a conventional three-electrode system. A platinum (Pt) was used as working electrode, a Pt wire as a counter electrode and with an Ag/Ag^+ reference electrode. Ferrocene/ferrocenium couple ($FeCp_2^+/FeCp_2^0$) was used as the internal standard. Potentials were referenced to $FeCp_2^+/FeCp_2^0$, which is −4.80 eV related to vacuum.

5.2 Stability

The solution phase photo-stability of the N-heteropentacenes have been studied by monitoring their attenuation of absorbance in dilute toluene solutions under air-saturated and ambient light (fluorescent light) conditions at room temperature, following the method described in literatures.[67-69] Thermogravimetric analyses (TGA) were carried out on a Linseis STA PT1600. A heating rate of 10 °C min^{-1} under flowing N_2 was used from room temperature to high temperature to investigate the thermal stabilities.

5.3 OFET device fabrication and characterization

A thermally grown dry silicon dioxide layer (400 nm) with a capacitance per unit area of 9.0×10^{-9} F/cm^2 functioned as the gate dielectric; while a heavily n-doped silicon substrate functioned as the gate electrode. Firstly, the substrates were immersed into hot sulfuric acid (98%) and hydrogen peroxide (v/v = 7:3) mixed solution for 30 minutes to get rid of organic compounds physically absorbed on the substrate. They were then successively cleaned with deionized water, isopropyl alcohol and acetone, and dried in a vacuum oven. OTMS treatment[23] was done by spin-coating a 3 mM solution of OTMS in trichloroethylene on a cleaned wafer, then the substrates were put in a closed container with a small vial containing a few millimeters of ammonia solution (25%~28% in H_2O) for 12 h at room temperature to accelerate hydrolysis of alkylsilanes and to promote bonding to SiO_2 surface.[70] The substrates were then rinsed with deionized water and sonicated in toluene for 10 minutes twice. The organic semiconductors were deposited at a rate below 0.1 Å s^{-1} under a pressure of 10^{-6} Torr to a final thickness of 50 nm as determined in-situ by a quartz crystal monitor. The fabrication was completed by depositing a layer of Au electrode on the organic films through a shadow mask to form top-contact bottom gate devices. The channel width (W) and the channel length (L) were 3000 μm and 150 μm respectively. OFETs measurements were performed in the argon glove box using a Keithley 4200 semiconductor parameter analyzer. Mobilities and threshold voltages of the thin film transistors were extracted from their transfer characteristics. Mobilities were calculated using the standard OFETs equation under saturation regime (Equation 3),

Journal of Materials Chemistry C Accepted Manuscript

This journal is © The Royal Society of Chemistry 2015

$$\mu = \frac{2L}{C_i W}\left(\frac{d\sqrt{I_{DS}}}{dV_G}\right)^2 \quad (3)$$

where μ stands for the field-effect mobility under saturation regime, C_i for the area capacitance of the gate dielectrics.
In this work, the thin film transistors were fabricated following standard procedure (top-contact OFET devices fabricated on OTMS-modified SiO_2 dielectric at T_{sub}= 60°C with Au electrodes and W/L=20).

5.4 X-ray diffraction

X-ray diffraction patterns of all pentacene derivatives thin films were obtained using PANalytical X PERT PRO. The thin films were deposited on OTMS/SiO_2/Si substrates at T_{sub} = 60 °C.

5.5 AFM images

AFM measurement were conducted using Agilent 5500 scanning probe microscope on the samples with a silicon tip, under tapping mode. Picoview software was used to handle the raw AFM images. Thin films deposited at T_{sub} = 60 °C on OTMS-treated SiO_2/Si were used for AFM studies. All AFM images were collected in air under ambient conditions. The topographic images were obtained from multiple samples based on same materials; and for each sample, different regions were scanned to ensure reproducibility.

Acknowledgements

This work is supported by National Basic Research Program of China (973 Program) No.2012CB933102, National Natural Science Foundation of China (NSFC. 21233001, 21190034, 21073079, J1103307, 21202176), Specialized Research Fund for the Doctoral Program of Higher Education (SRFDP. 20110211130001) and the 111 Project.

Notes

[a] State Key Laboratory of Applied Organic Chemistry (SKLAOC)
College of Chemistry and Chemical Engineering
Key Laboratory of Special Function Materials and Structure Design, Ministry of Education
Lanzhou University, Lanzhou, 730000, China
Corresponding Author:
E-mails: Haoli.zhang@lzu.edu.cn
[b] School of Physical Science and Technology
Lanzhou University, Lanzhou, 730000, China
[c] State Key Laboratory for Oxo Synthesis & Selective Oxidation
Lanzhou Institute of Chemical Physics, CAS
Lanzhou 730000, China
[d] Department of Polymer Engineering
College of Polymer Science and Engineering
The University of Akron
Akron, Ohio 44236, United States

are included in the supporting information.

Electronic Supplementary Information (ESI) available: Synthesis and detailed characterization data such as spectroscopic and electrochemical properties, stability, X-ray diffraction patterns, 2D-GIXRD patterns, AFM images, FET characterization, and simulation of charge transport within single crystals and disordered films. See DOI: 10.1039/b000000x/

References

1. C. Wang, H. Dong, W. Hu, Y. Liu and D. Zhu, *Chem. Rev.*, 2012, 112, 2208.
2. Y. Wen, Y. Liu, Y. Guo, G. Yu and W. Hu, *Chem. Rev.*, 2011, 111, 3358.
3. J. Zaumseil and H. Sirringhaus, *Chem. Rev.* , 2007, 107, 1296.
4. V. Coropceanu, J. Cornil, D. A. d. S. Filho, Y. Olivier, R. Silbey and J.-L. Brédas, *Chem. Rev.*, 2007, 107, 926.
5. A. R. Murphy and J. M. J. Fréchet, *Chem. Rev.*, 2007, 107, 1066.
6. J. E. Anthony, *Angew. Chem. Int. Ed.*, 2008, 47, 452.
7. G. Giri, E. Verploegen, S. C. B. Mannsfeld, S. Atahan-Evrenk, D. H. Kim, S. Y. Lee, H. A. Becerril, A. n. Aspuru-Guzik, M. F. Toney and Z. Bao, *Nature*, 2011, 480, 504.
8. F. Zhang, Y. Hu, T. Schuettfort, C.-a. Di, X. Gao, C. R. McNeill, L. Thomsen, S. C. B. Mannsfeld, W. Yuan, H. Sirringhaus and D. Zhu, *J. Am. Chem. Soc.*, 2013, 135, 2338.
9. J. Mei, Y. Diao, A. L. Appleton, L. Fang and Z. Bao, *J. Am. Chem. Soc.*, 2013, 135, 6724.
10. R. Schmidt, J. H. Oh, Y.-S. Sun, M. Deppisch, A.-M. Krause, K. Radacki, H. Braunschweig, M. Könemann, P. Erk, Z. Bao and F. Würthner, *J. Am. Chem. Soc.*, 2009, 131, 6215.
11. K. C. Dickey, J. E. Anthony and Y.-L. Loo, *Adv. Mater.* , 2006, 18, 1721.
12. C. Liu, C. Xiao, Y. Li, W. Hu, Z. Li and Z. Wang, *Chem. Commun.*, 2014, 50, 12462.
13. E. J. Meijer, D. M. d. Leeuw, S. Setayesh, E. v. Veenendaal, B.-H. Huisman, P. W. M. Blom, J. C. Hummelen, U. Scherf and T. M. Klapwijk, *Nat. Mater.*, 2003, 2, 678.
14. T. B. Singh, F. Meghdadi, S. Gunes, N. Marjanovic, G. Horowitz, P. Lang, S. Bauer and N. S. Sariciftci, *Adv. Mater.*, 2005, 17, 2315.
15. T. Takahashi, T. Takenobu, J. Takeya and Y. Iwasa, *Appl. Phys. Lett.*, 2006, 88, 033503.
16. H. Usta, A. Facchetti and T. J. Marks, *J. Am. Chem. Soc.*, 2008, 130, 8580.
17. F. Cicoira and C. Santato, *Adv. Funct. Mater.*, 2007, 17, 3421.
18. Y. Suzuki, E. Miyazaki and K. Takimiya, *J. Am. Chem. Soc.*, 2010, 132, 10453.
19. Y. Ie, M. Nitani, M. Karakawa, H. Tada and Y. Aso, *Adv. Funct. Mater.*, 2010, 20, 907.
20. X. Gao, C.-a. Di, Y. Hu, X. Yang, H. Fan, F. Zhang, Y. Liu, H. Li and D. Zhu, *J. Am. Chem. Soc.*, 2010, 132, 3697.
21. Z. Liang, Q. Tang, J. Liu, J. Li, F. Yan and Q. Miao, *Chem. Mater.*, 2010, 22, 6438.
22. M. L. Tang and Z. Bao, *Chem. Mater.*, 2011, 23, 446.
23. M. L. Tang, J. H. Oh, A. D. Reichardt and Z. Bao, *J. Am. Chem. Soc.* , 2009, 131, 3733.
24. M. Winkler and K. N. Houk, *J. Am. Chem. Soc.*, 2007, 129, 1805.
25. X.-K. Chen, L.-Y. Zou, J.-X. Fan, S.-F. Zhang and A.-M. Ren, *Org. Electron.*, 2012, 13, 2832.
26. A. L. Appleton, S. M. Brombosz, S. Barlow, J. S. Sears, J.-L. Brédas, S. R. Marder and U. H. F. Bunz, *Nat. Commun.*, 2010, 1, 1.
27. Q. Miao, T.-Q. Nguyen, T. Someya, G. B. Blanchet and C. Nuckolls, *J. Am. Chem. Soc.*, 2003, 125, 10284.
28. U. H. F. Bunz, *Chem. Eur. J.* , 2009, 15, 6780.

Journal of Materials Chemistry C Accepted Manuscript

29. X. Xu, B. Shan, S. Kalytchuk, M. Xie, S. Yang, D. Liu, S. V. Kershaw and Q. Miao, *Chem. Commun.*, 2014, 50, 12828.
30. Y.-Y. Liu, C.-L. Song, W.-J. Zeng, K.-G. Zhou, Z.-F. Shi, C.-B. Ma, F. Yang, H.-L. Zhang and X. Gong, *J. Am. Chem. Soc.*, 2010, 132, 16349.
31. Z. Liang, Q. Tang, J. Xu and Q. Miao, *Adv. Mater.*, 2011, 23, 1535.
32. G. Li, Y. Wu, J. Gao, C. Wang, J. Li, H. Zhang, Y. Zhao and Q. Zhang, *J. Am. Chem. Soc.*, 2012, 134, 20298.
33. J. Li, P. Li, J. Wu, J. Gao, W. W. Xiong, G. Zhang, Y. Zhao and Q. Zhang, *J. Org. Chem.*, 2014, 79, 4438.
34. G. Li, Y. Wu, J. Gao, J. Li, Y. Zhao and Q. Zhang, *Chem. Asian. J.*, 2013, 8, 1574.
35. G. Li, J. Miao, J. Cao, J. Zhu, B. Liu and Q. Zhang, *Chem. Commun.*, 2014, 50, 7656.
36. P. Y. Gu, F. Zhou, J. Gao, G. Li, C. Wang, Q. F. Xu, Q. Zhang and J. M. Lu, *J. Am. Chem. Soc.*, 2013, 135, 14086.
37. C.-L. Song, C.-B. Ma, F. Yang, W.-J. Zeng, H.-L. Zhang and X. Gong, *Org. Lett.*, 2011, 13, 2880.
38. W.-J. Zeng, X.-Y. Zhou, X.-J. Pan, C.-L. Song and H.-L. Zhang, *AIP Advances.*, 2013, 3, 012101.
39. C. D. Sheraw, T. N. Jakson, D. L. Eaton and J. E. Anthony, *Adv. Mater.*, 2003, 15, 2009.
40. T. Heim, K. Lmimouni and D. Vuillaume, *Nano. Lett.*, 2004, 4, 2145.
41. V. Coropceanu, H. Li, P. Winget, L. Zhu and J.-L. Brédas, *Annu. Rev. Mater. Res.*, 2013, 43, 63.
42. M. L. Tang, A. D. Reichardt, P. Wei and Z. Bao, *J. Am. Chem. Soc.*, 2009, 131, 5264.
43. J. Gao, R. Li, L. Li, Q. Meng, H. Jiang, H. Li and W. Hu, *Adv. Mater.*, 2007, 19, 3008.
44. H. Usta, C. Risko, Z. Wang, H. Huang, M. K. Deliomeroglu, A. Zhukhovitskiy, A. Facchetti and T. J. Marks, *J. Am. Chem. Soc.*, 2009, 131, 5586.
45. C. R. Swartz, S. R. Parkin, J. E. Bullock, J. E. Anthony, A. C. Mayer and G. G. Malliaras, *Org. Lett.*, 2005, 7, 3163.
46. C.-L. Sun, J. Li, H.-W. Geng, H. Li, Y. Ai, Q. Wang, S.-L. Pan and H.-L. Zhang, *Chem. Asian. J.*, 2013, 8, 3091.
47. J. E. Anthony, J. S. Brooks, D. L. Eaton and S. R. Parkin, *J. Am. Chem. Soc.*, 2001, 123, 9482.
48. D. Braga and G. Horowitz, *Adv. Mater.*, 2009, 21, 1473.
49. R. W. I. d. Boer, M. E. Gershenson, A. F. Morpurgo and V. Podzorov, *phys. stat. sol. (a)*, 2004, 201, 1302.
50. M. Zhang, J. Knoch, S.-L. Zhang, S. Feste, M. Schr¨oter and S. Mantl, *IEEE Trans. Electron Device,*, 2008, 55, 858.
51. J.-L. Brédas, D. Beljonne, V. Coropceanu and J. Cornil, *Chem. Rev.*, 2004, 104, 4971.
52. L. Wang, G. Nan, X. Yang, Q. Peng, Q. Li and Z. Shuai, *Chem. Soc. Rev.*, 2010, 39, 423.
53. D. Moia, V. Vaissier, I. López-Duarte, T. Torres, M. K. Nazeeruddin, B. C. O'Regan, J. Nelson and P. R. F. Barnes, *Chem. Sci.*, 2014, 5, 281.
54. Z. Shuai, H. Geng, W. Xu, Y. Liao and J. M. Andre, *Chem. Soc. Rev.*, 2014, 43, 2662.
55. N. Metropolis, A. W. Rosenbluth, M. N. Rosenbluth, A. H. Teller and E. Teller, *J. Chem. Phys.*, 1953, 21, 1087.
56. J. J. Kwiatkowski, J. Nelson, H. Li, J. L. Brédas, W. Wenzelc and C. Lennartzd, *Phys. Chem. Chem. Phys.* , 2008, 10, 1852.
57. V. Rühle, A. Lukyanov, F. May, M. Schrader, T. Vehoff, J. Kirkpatrick, B. o. Baumeier and D. Andrienko, *J. Chem. Theory Comput.*, 2011, 7, 3335.
58. W.-Q. Deng and I. William A. Goddard, *J. Phys. Chem. B*, 2004, 108, 8614.
59. G. Nan, X. Yang, L. Wang, Z. Shuai and Y. Zhao, *Phys. Rev. B*, 2009, 79, 115203.
60. K. Senthilkumar, F. C. Grozema, F. M. Bickelhaupt and L. D. A. Siebbeles, *J. Chem. Phys.*, 2003, 119, 9809.
61. M. C. R. Delgado, K. R. Pigg, D. A. d. S. Filho, N. E. Gruhn, Y. Sakamoto, T. Suzuki, R. M. Osuna, J. Casado, V. Hernández, J. T. L. Navarrete, N. G. Martinelli, J. Cornil, R. S. Sánchez-Carrera, V. Coropceanu and J.-L. Brédas, *J. Am. Chem. Soc.*, 2009, 131, 1502.
62. H. Geng, Y. Niu, Q. Peng, Z. Shuai, V. Coropceanu and J. L. Brédas, *J. Chem. Phys.*, 2011, 135, 104703.
63. J. L.Brédas, J. P.Calbert, D. A. d. S. Filho and J.Cornil, *Proc Natl Acad Sci USA.*, 2002, 99, 5804.
64. C.-H. Li, C.-H. Huang and M.-Y. Kuo, *Phys. Chem. Chem. Phys.* , 2011, 13, 11148.
65. H. Li, R. Zheng and Q. Shi, *J. Phys. Chem. C*, 2012, 116, 11886.
66. V. T. T. Huong, H. T. Nguyen, T. B. Tai and M. T. Nguyen, *J. Phys. Chem. C*, 2013, 117, 10175.
67. J. Wang, K. Liu, Y.-Y. Liu, C.-L. Song, Z.-F. Shi, J.-B. Peng, H.-L. Zhang and X.-P. Cao, *Org. Lett.*, 2009, 11, 2563.
68. A. Maliakal, K. Raghavachari, H. Katz, E. Chandross and T. Siegrist, *Chem. Mater.* , 2004, 16, 4980.
69. H. Qu and C. Chi, *Org. Lett.*, 2010, 12, 3360.
70. Y. Ito, A. A. Virkar, S. Mannsfeld, J. H. Oh, M. Toney, J. Locklin and Z. Bao, *J. Am. Chem. Soc.*, 2009, 131, 9396.

Journal of Materials Chemistry C Accepted Manuscript

This journal is © The Royal Society of Chemistry 2015

Journal of Materials Chemistry C Accepted Manuscript

FULL PAPER

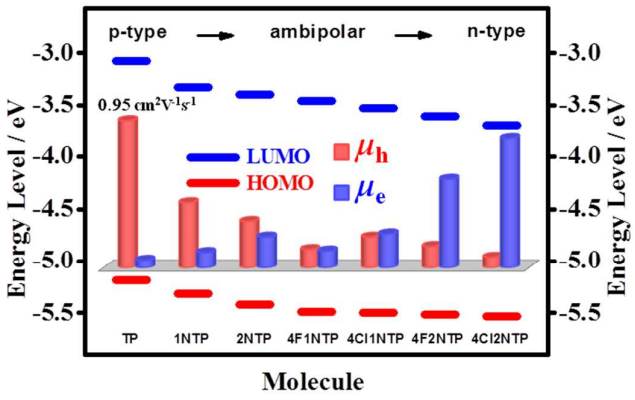

Organic Semiconductors

*K. Liu, C.-L. Song, Y.-C. Zhou, X.–Y. Zhou, X.–J. Pan, L.–Y. Cao, C. Zhang, Y. Liu, X. Gong & H.-L. Zhang**

■■ – ■■

Tuning the Ambipolar Charge Transport Properties of N-heteropentacenes by Their Frontier Molecular Orbital Energy Levels

Tuning the Ambipolar Performance: Carefully designed N-heteropentacenes realized a fine tune of their HOMOs and LUMOs, which dramatically affected their ambipolar transport performance (hole/electron mobilities and threshold voltages) in field-effect transistors.